Icarus 254 (2015) 150–156

Contents lists available at ScienceDirect

Icarus

journal homepage: www.elsevier.com/locate/icarus

# Asteroid (90) Antiope: Another icy member of the Themis family?

Kelsey D. Hargrove [a,*], Joshua P. Emery [b], Humberto Campins [a], Michael S.P. Kelley [c]

[a] Physics Department, University of Central Florida, Orlando, FL 32816, United States
[b] Earth and Planetary Science Dept. and Planetary Geosciences Institute, University of Tennessee, Knoxville, TN 37996, United States
[c] Department of Astronomy, University of Maryland, College Park, MD 20742-2421, United States

ARTICLE INFO

*Article history:*
Received 27 October 2014
Revised 23 February 2015
Accepted 8 March 2015
Available online 14 March 2015

*Keywords:*
Asteroids
Asteroids, surfaces
Asteroids, composition
Infrared observations
Ices, IR spectroscopy

ABSTRACT

Many members of the Themis family show evidence of hydration in the form of oxidized iron in phyllosilicates (Florczak, M. et al. [1999]. Astron. Astrophys. Suppl. Ser. 134, 463–471), and OH-bearing minerals (Takir, D., Emery, J.P. [2012]. Icarus 219, 641–654). The largest member, (24) Themis, has $H_2O$ ice covering its surface (Campins, H. et al. [2010]. Nature 464, 1320–1321; Rivkin, A.S., Emery, J.P. [2010]. Nature 464, 1322–1323). We have investigated the second largest Themis-family asteroid, (90) Antiope, which Castillo-Rogez and Schmidt (Castillo-Rogez, J.C., Schmidt, B.E. [2010]. Geophys. Res. Lett. 37, L10202) predict to have a composition that includes water ice and organics. We obtained 2–4-μm spectroscopy of (90) Antiope in 2006 and 2008, and we find an absorption in the 3-μm region clearly present in our 2008 spectrum and likely in our 2006 spectrum. Both spectra have rounded, bowl-shaped absorptions consistent with those ascribed to water ice as in the spectrum of Asteroid (24) Themis. We also present and compare Spitzer 8–12-μm mid-infrared spectra of (24) Themis and (90) Antiope. We find that (90) Antiope is lacking a "fairy castle" dusty surface, which is in contrast to (24) Themis, other Themis family members (Licandro, J. et al. [2012]. Astron. Astrophys. 537, A73), and Jupiter Trojans (e.g. Emery, J.P., Cruikshank, D.P., Van Cleve, J. [2006]. Icarus 182, 496–512). We conclude that the surface structure of (90) Antiope is most similar to Cybele Asteroid (121) Hermione (Hargrove, K.D. et al. [2012]. Icarus 221, 453–455).



## 1. Introduction

The Themis family (Zappala et al., 1995) is comprised of dark, compositionally primitive bodies. Themis members are mainly Tholen and Barucci (1989) C- and B-taxonomic types (Florczak et al., 1999), and in the Bus taxonomy (Bus and Binzel, 2002) they are largely C-complex with a few members belonging to the X-complex (Mothé-Diniz et al., 2005).

This population resides in the outer Main Belt where hydration has been observed in the form of oxidized iron in phyllosilicates (Florczak et al., 1999), hydroxyl-bearing minerals (Takir and Emery, 2012) and water ice (Campins et al., 2010; Rivkin and Emery, 2010). In particular, near-infrared spectral features in the 3-μm range have been detected in three members of the Themis family, sampling both the "sharp" and "rounded" variations of the absorption (Takir and Emery, 2012). This absorption has also been detected in the spectra of several other outer belt asteroids, including six in the Cybele group and three in the Hilda group (Licandro et al., 2011; Hargrove et al., 2012; Takir and Emery, 2012).

The sharp 3-μm absorption is produced by the fundamental stretch vibration of hydroxyl, and is diagnostic of OH incorporated into a mineral lattice or at interlayer sites (Jones, 1988). This feature has a band minimum at 2.7 μm, though, in ground-based near-infrared spectra, this minimum is obscured by the strong telluric absorptions between ~2.5–2.9 μm. The detectable part of this feature rises linearly from about 2.9 μm to approximately 3.2 μm, producing a sharp "checkmark" appearance. Several asteroids thus far have this signature, including Themis-family asteroid (104) Klymene (Takir and Emery, 2012). Spectral features showing hydration in the Themis family are not surprising considering that roughly 50% of its members show signs of aqueous alteration in their visible spectra (Florczak et al. (1999)), and currently four so-called Main-Belt comets (MBCs) belong to this family (or the Beagle sub-family; e.g. Haghighipour (2009), Hsieh et al. (2012) and Hsieh (2014)).

The rounded 3-μm feature is caused by the symmetric stretch of the $H_2O$ molecule in water ice, and has a band minimum at 3.1 μm.

* Corresponding author.
*E-mail address:* khargrove@knights.ucf.edu (K.D. Hargrove).

http://dx.doi.org/10.1016/j.icarus.2015.03.008
0019-1035/

Water ice has been observed on several asteroids, including (24) Themis (Campins et al., 2010; Rivkin and Emery, 2010), the largest member of the Themis family. In their study of 28 outer-belt asteroids ($\sim$2.6 < $a$ < $\sim$4 AU) Takir and Emery (2012) found that most asteroids with this rounded absorption are concentrated in the 3.4 < $a$ < 4.0 AU region, and may represent objects that did not experience sufficient thermal processing to induce aqueous alteration; however, the models of Castillo-Rogez and Schmidt (2010) predict that many other Themis-family asteroids ($\sim$3.1 < $a$ < $\sim$3.2 AU) contain water ice, and only three of these have been investigated thus far in the 2–4-μm region: 24 Themis, 90 Antiope (this work) and 104 Klymene. It is possible that the clustering of these icy objects found by Takir and Emery (2012) beyond 3.4 AU may, with further observations, expand to include objects at shorter heliocentric distances, especially within the Themis family.

### 1.1. Asteroid (90) Antiope

Themis family member (90) Antiope is a unique and puzzling object. It is part of a binary system with a companion almost equal in size. These two objects, (90) Antiope and S/2000 (90) 1 (henceforth companion), are among the five hundred largest asteroids (Descamps et al., 2007) with WISE diameters of 124 km and 119 km (Masiero et al., 2011), respectively, and are two of the largest objects in the Themis family. Antiope has a visible and near-infrared reflectance spectrum typical of C-type asteroids, consistent with some but not all other Themis members,[1] characterized by a linear, featureless spectrum in the 0.5–2.5-μm region with a small positive slope beginning around 1.1 μm (DeMeo et al., 2009). Marchis et al. (2011) has determined that both Antiope and its companion share this C (possibly Cb) taxonomic type.

Based on (90) Antiope's low bulk density of 1.28 g/cm$^3$ (Descamps et al., 2007), Castillo-Rogez and Schmidt (2010) suggest this asteroid is a collisional remnant of a proto-Themis object that was enveloped in an icy shell totaling $\sim$50% of its volume. They argue that Antiope, its companion, and other large Themis family objects may be comprised of a large fraction of the parent body's ice shell. Their models also suggest that the ice on these asteroids may not be completely pure, possibly contaminated with organics, brines, other hydrated minerals, and oxides.

Using component-resolved near-infrared spectroscopy in the $\sim$1.1–2.4-μm region, Marchis et al. (2011) found that the spectra of (90) Antiope and its companion do not show any detectable broad water ice absorptions at 1.25, 1.52, and 2.02 μm. Interestingly, these features are not detectable in the case of Asteroid (24) Themis, yet this asteroid has an icy surface evident from its feature at 3.1 μm (Campins et al., 2010; Rivkin and Emery, 2010). This is not surprising considering ice features at the shorter wavelengths tend to be significantly weaker in strength, especially if the albedo of the ice is lowered by a spectrally neutral contaminant. Thus Marchis et al. (2011) suggest spectra at wavelengths longer than 2.5 μm are needed to test for the presence of water ice on (90) Antiope.

In this work, we continue our characterization of Themis family asteroids in the 2–4-μm region. We present near-infrared reflectance spectra of Asteroid (90) Antiope. To investigate the nature of hydration on this body, we determine the presence and shape of the 3-μm spectral feature, which is diagnostic of surface composition and thermal history. In addition, we compare and contrast the 5–14-μm emission spectrum, which can also be diagnostic of surface properties, of (90) Antiope with that of Asteroid (24) Themis, also known to exhibit a similar 3-μm feature.

[1] Several Themis members have B-, Cb- and Ch-type spectra in the visible and near-infrared (e.g. Mothé-Diniz et al., 2005; Ziffer et al., 2011; De Leon et al., 2012).

## 2. Observations and data reduction

### 2.1. IRTF near-infrared spectra

We observed (90) Antiope using the NASA Infrared Telescope Facility (IRTF), a 3.0-m telescope at Mauna Kea Hawaii. In Table 1 we list all of our observing details. We present two independent spectra of (90) Antiope, the first of which we obtained on the night of July 23, 2006. To correct for telluric absorption and to achieve relative reflectance spectra we observed HD 14786, a near-solar spectral type (G5) star. This night had high clouds and seeing of roughly 0.7 arcsec. We later observed (90) Antiope on the night of January 23, 2008, as well as the solar analog star HD 28099 (de Strobel, 1996), and the standard star BS 2962. This second night was photometric with good transparency and a seeing of approximately 0.6 arcsec.

For all our observations, we used the SpeX cryogenic spectrograph/imager (Rayner et al., 2003). We selected the Long Cross-dispersed (LXD) 1.9 mode that produced medium-resolution spectra in the 1.9–4.2-μm wavelength range. We chose the 0.8 × 15 arcsec slit with an image scale of 0.15 arcsec/pixel that resulted in a spectral resolution $\lambda/\Delta\lambda$ of $\sim$800, which we later binned to a resolution $\lambda/\Delta\lambda$ of $\sim$300 to maximize the signal-to-noise while preserving an appropriate spectral resolution. We obtained the spectra in A–B (object-sky) pairs by nodding the telescope 10 arcsec along the long dimension of the slit. The slit was oriented perpendicular to the horizon. We calibrated and reduced our spectra using the IDL-based spectral reduction program Spextool (v3.4) (Cushing et al., 2004). First, Spextool removed emission from atmospheric OH and thermal emission from both the sky and telescope by calculating the difference between the A–B pairs. The resulting images of this subtraction were then divided by normalized flat field images. Spextool extracted the asteroid and star spectra by adding the flux for each channel within an aperture size defined by the user, which in this case was 10 pixels wide. For LXD modes Spextool performs wavelength calibration by using a combination of emission lines from an Argon calibration lamp for shorter wavelengths and sky OH emission lines for longer wavelengths, since the number and intensity of Argon emission lines diminish rapidly longward of 3.0 μm where OH emission lines are plentiful (Cushing et al., 2004).

All of our ground-based spectra were contaminated with telluric features from Earth's atmosphere. These strong features of $H_2O$ and $CO_2$ can vary in depth depending on the local precipitable water vapor and airmass of the object. Therefore, we generated atmospheric transmission profiles for the nights of our observations using the IDL routine ATRAN (Lord, 1992) that modeled then removed these telluric features from our asteroid and star spectra. The routine then divided each corrected asteroid spectrum by both the corrected solar analog and standard star spectra. These asteroid/solar analog and asteroid/standard star spectra were median combined into a single spectrum. The final spectrum of the 2006 observation of Asteroid (90) Antiope was comprised of 30 A–B pairs, and the 2008 observation of 29 A–B pairs.

Longward of $\sim$3.3 μm both spectra of (90) Antiope show an increase in reflectance caused by the combination of both reflected light and thermal radiation from its surface. We modeled this thermal component using the Near-Earth Asteroid Thermal Model (Harris, 1998), and removed it from our near-infrared spectra. We used the diameter and beaming parameter determined from modeling the mid-infrared spectra of (90) Antiope (see Section 4) to model the thermal component in the near-infrared. The thermal

**Table 1**
Details of the IRTF and Spitzer observations, including the object's distance to the Sun ($r$) and the Earth ($\Delta$), and its phase angle ($\alpha$) at the time of our observations. The exposure time for IRTF observations is the total on source integration time. The exposure time for Spitzer observations is the total integration time for all DCEs centered on the object for the SL module (see details in main text).

| Object | Telescope | UT start | Time (UT) | $r$ (AU) | $\Delta$ (AU) | $\alpha$ (deg) | Total time (s) | Pipeline version |
|---|---|---|---|---|---|---|---|---|
| 90 Antiope | IRTF | 2006-January-23 | 14:40:23 | 2.87 | 2.80 | 20.6 | 1520 | – |
| 90 Antiope | IRTF | 2008-July-23 | 07:16:54 | 3.58 | 2.65 | 6.0 | 2480 | – |
| 24 Themis | Spitzer | 2009-April-25 | 01:28:11 | 3.54 | 3.37 | 16.6 | 25 | S18.7.0 |
| 90 Antiope | Spitzer | 2004-July-12 | 23:31:20 | 3.16 | 3.04 | 18.7 | 130 | S18.18.0 |

contribution for the 2006 observation of (90) Antiope was approximately 2% at 3.5 μm and 6% at 3.8 μm, and for the 2008 observation <1% at 3.5 μm and 1% at 3.8 μm. The onset and amount of the thermal components for these two spectra are consistent with the different heliocentric distances (Table 1), and thus surface temperatures, of (90) Antiope during our observations. Since the onset of the thermal component is longward of 3.3 μm for both observations it does not affect our interpretation of the 3-μm features discussed in Section 3.

### 2.2. Spitzer/IRS mid-infrared spectra

The mid-infrared spectra were obtained with NASA's Spitzer Space Telescope (Werner et al., 2004) Infrared Spectrograph (IRS) instrument (Houck et al., 2004). The observational details are also outlined in Table 1. For both (24) Themis and (90) Antiope IRS acquired spectra in mapping mode, resulting in a grid of map positions around the central target position with spectra obtained at each position. For Themis, IRS obtained spectra in the short-wavelength low-resolution (SL) mode (SL2: 5.1–7.6 μm, SL1: 7.5–14.3 μm, and SL3: 7.3–8.7 μm), short-wavelength high-resolution (SH) mode (9.9–19.6 μm), and long-wavelength high-resolution (LH) mode (18.7–37.2 μm). Combined these modules provide a resolution $R$ ~60–600 over the spectral range of ~5–38 μm. For (90) Antiope IRS also observed this asteroid in the SL, SH, and LH modes, though the necessary background observations for the SH and LH modes were not obtained. Therefore, we limit our interpretation of the mid-infrared spectra of Themis and Antiope to the ~5–14-μm range with a resolution $R$ ~60–128.

Both asteroids had a spectral map consisting of 2 steps parallel to the long dimension of the slit (57″) and 3 steps perpendicular (3.6–3.7″), though we selected the mapping steps that were most centered on the asteroid. Before extracting the spectra, we performed a basic background subtraction on the Basic Calibrated Data using background frames constructed from off-source slits. For example, to create the background for the SL1 position 1, we averaged the frames from SL1 position 2, SL2 position 1 and SL2 position 2. To combine the output uncertainty files we added the frames in quadrature, and combined the mask files pixel-by-pixel using the bitwise-or method. We extracted the spectra using SPICE (Spitzer IRS Custom Extraction) software[2] choosing the point-source option and the regular extraction method. To address the order-to-order mismatch in the reduced spectra of Themis and Antiope, we scaled the SL2 order to align with the SL1 order by 1.097 and 0.087, respectively. We determined these scale amounts by fitting extended, low-order polynomials to each disjointed order then determined the scale factor with the lowest chi-square value that best joined the data in the overlap regions. Our scale factors are consistent with the IRS pipeline's absolute calibration uncertainty of ⩽10%.

In addition to the offsets between modes there is an artifact that affects our SL1 spectra, known as the 14-μm teardrop. This artifact typically produces excess flux in the 13.5–15.0-μm region that closely resembles an emission feature. Since there is no way to characterize the behavior of the teardrop, there is no way to correct for it. Therefore, we have chosen to remove this region from the SL1 order.

## 3. IRTF near infrared spectra

Our two independent spectra of Themis family Asteroid (90) Antiope are presented in Fig. 1, with an estimate of the continuum for each observation. Our spectrum of Asteroid (24) Themis, also obtained with the IRTF and published in Campins et al. (2010), is shown for comparison. We calculated the spectral continua by extrapolating the slope in the K-band region (1.95–2.5 μm) using IRTF 0.8–2.5-μm near-infrared spectra of Antiope and Themis that are part of the MIT-UH-IRTF Joint Campaign for NEO Reconnaissance.[3] Our 2006 and 2008 2–4-μm spectra exhibit an absorption below the continuum from approximately 2.9–3.2 μm that is consistent with an absorption due to surface ice or hydroxyl. Qualitatively the absorption appears rounded and bowl-shaped, similar to the 3.1-μm ice feature in the spectrum of (24) Themis. Thus, we have ruled out the steep, linearly rising "checkmark" feature that also appears in the 2.9–3.2-μm region seen in, for example, the spectrum of (104) Klymene (Takir and Emery, 2012) and (121) Hermione (Hargrove et al., 2012; Takir and Emery, 2012).

To further investigate the nature of (90) Antiope's absorption, we compared Antiope with the same spectral model presented in Rivkin and Emery (2010; their Fig. 1) to describe the 3-μm feature of (24) Themis. This spectral "ice" model consists of an intimate mixture of 29% pyroxene coated with a 0.045-μm-thick layer of water ice and 71% amorphous carbon. Fig. 2 shows our 2006 and 2008 spectra of (90) Antiope compared with (24) Themis from Campins et al. (2010), and the Themis ice model from Rivkin and Emery (2010). We have divided the asteroid spectra by their continua to remove any slopes, and we normalized the ice models at 3.1 μm for each dataset. Our 2006 spectrum has the lowest $S/N$ and does not appear to necessarily match the width, shape and depth of the ice model, especially in the 2.9–3.0-μm region. Therefore, it is inconclusive if the Themis ice model is appropriate to describe this particular dataset. Our 2008 spectrum has improved $S/N$, and these data follow the shape of the ice model in the 2.9–3.1-μm region more closely. Comparing with Themis, neither Antiope spectra are entirely consistent with the ice model in the full 2.9–3.2-μm region. This may be due to the $S/N$ of our data and/or the ice model, which was generated for (24) Themis, and may not be sufficient for the absorption we detect in the spectra of (90) Antiope.

When studying hydration features in the 3-μm region it is relevant to mention the 0.7-μm feature, another indicator of hydration, as many asteroids show evidence of both absorptions (e.g. Vilas, 1994; Rivkin et al., 2002; Howell et al., 2011). Of the nine primitive asteroids with known rounded 3.1-μm features, none thus far show conclusive evidence of a 0.7-μm absorption indicative of the $Fe^{2+} \rightarrow Fe^{3+}$ charge transfer transition of oxidized iron in phyl-

[2] http://irsa.ipac.caltech.edu/data/SPITZER/docs/dataanalysistools/tools/spice/.

[3] http://smass.mit.edu/minus.html.

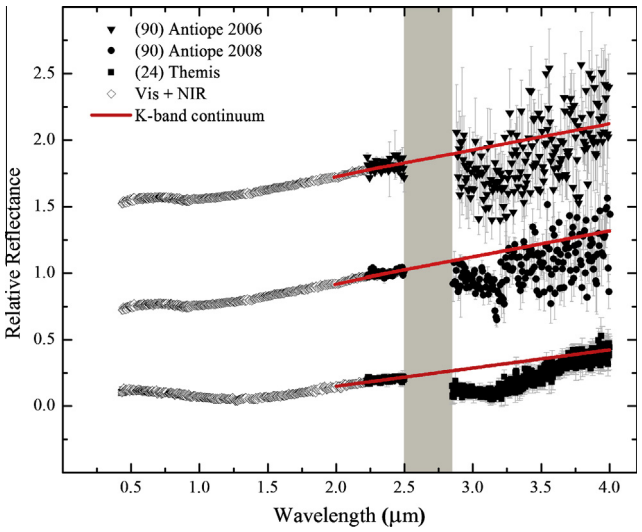


**Fig. 1.** Our two independent observations of Asteroid (90) Antiope, obtained with the IRTF, rebinned to a resolution of 0.006 μm, and offset for clarity. The error bars are the standard deviation of the flux in each spectral bin. Both observations indicate an absorption below the continuum in the 3-μm region. The top data set is the rebinned relative reflectance spectrum of (90) Antiope observed July 23, 2006 at 0.42 orbital phase. The middle spectrum was observed January 23, 2008 at approximately at 0.90 orbital phase. The bottom spectrum is that of Asteroid (24) Themis, the largest member of the Themis family, and an asteroid with a confirmed detection of water ice (Campins et al., 2010). The solid gray box indicates the region of strong telluric absorptions that we removed from our asteroid spectra. The 0.8–2.5-μm spectra are from the MIT-UH-IRTF survey[3].

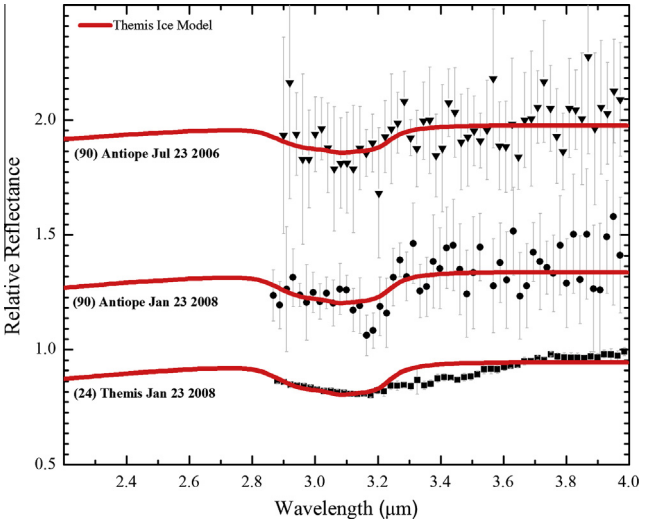


**Fig. 2.** Our two independent (90) Antiope spectra compared with Asteroid (24) Themis from Campins et al. (2010), and the ice model from Rivkin and Emery (2010). We rebinned our Antiope spectra to a resolution of 0.02 μm, and the error bars are the standard deviation of the flux in each spectral bin. All asteroid spectra have been divided by a continuum we extrapolated from the slope of their spectrum in the K-band region (1.95–2.5 μm). The ice model consists of a mixture of ice-coated amorphous carbon and pyroxene grains originally fit to (24) Themis in Rivkin and Emery (2010; shown in their Fig. 1), and we have normalized these models at 3.1 μm.

losilicates. The presence of this feature in the visible spectra of (90) Antiope is also unclear. Florczak et al. (1999), using the criterion defined by Vilas et al. (1993), detected a 0.7-μm absorption in the visible spectrum of Antiope from the S3OS2 survey (Lazzaro et al., 2004). However, this feature was not detected in the SMASS 0.44–0.92-μm spectrum (Bus and Binzel, 2002) of this asteroid, hence its classification among C-type asteroids, which are characterized by a featureless spectrum longward of 0.55 μm (i.e., they do not typically have 0.7-μm absorptions). Lazzaro et al. (2004) applied the classification methods of Tholen and Barucci (1989) and Bus and Binzel (2002) to the S3OS2 spectrum of (90) Antiope, classifying it as a Tholen Caa-type (a Tholen C-type with evidence of a broad aqueous alteration feature), and a Bus Ch-type (exhibiting a 0.7-μm absorption). Recently, Fornasier et al. (2014) reanalyzed the spectra of (90) Antiope from Lazzaro et al. (2004), confirming the presence of a 0.7-μm feature (0.73 μm ± 0.003 μm). However the authors note that for several asteroids, including (90) Antiope, a 0.7-μm feature is seen in some datasets and not in others, and this may be due to noise, differences in observational uncertainties, differences in data acquisition and reduction, or possibly variations in the surface composition.

Interestingly, there is evidence for a giant crater on the surface of (90) Antiope or its companion (between ~0.35 and 0.50 orbital phase; Descamps et al., 2009), and this could be a source of such compositional variations. During our 2006 observation, we observed a part of (90) Antiope's orbital phase (0.42–0.43 ± 0.04) where this large ~68 km crater may exist. We determined the orbital phase we observed by taking zero phase to be June 8.3804 UTC (Descamps et al., 2009), and using Antiope's rotational period of 16.5051 ± 0.0001 h (Descamps et al., 2007). This crater on (90) Antiope or its companion occupies roughly 70% of its average diameter and has a diameter/depth ratio of $t = 3$, suggesting this asteroid system has very low density and porous surface structure (Descamps et al., 2009).

Although compositional variations between Antiope and its companion were not found by Marchis et al. (2011) in the ~1.1–2.4-μm region, perhaps it is possible these exist in the 2–4-μm region. Does the deep, shadowed crater harbor more ice than the rest of the surface? Like Themis, are there widespread organics on the surface of Antiope? For us to answer these questions we need higher-$S/N$ rotationally resolved spectra of this asteroid system in the 2–4-μm region, especially between ~0.35–0.50 orbital phase.

## 4. Thermal model

To interpret the mid-infrared thermal emission of (90) Antiope and (24) Themis in terms of physical parameters we used the Near-Earth Asteroid Thermal Model (Harris, 1998), a refinement of the Standard Thermal Model (STM; Lebofsky and Spencer, 1989). The NEATM uses thermal infrared data at multiple wavelengths in order to estimate the diameter ($D$) and beaming parameter ($\eta$). Our inputs to the NEATM include the object's distance to the Sun ($r$) and Spitzer ($\Lambda$), and its phase angle ($\alpha$) at the time of the Spitzer observations. We calculated these values using the online ephemeris generator[4] provided by NASA's Jet Propulsion Laboratory. We obtained the slope parameter ($G$; Bowell et al., 1989) and the visible magnitude ($H$) from the WISE Main Belt Asteroid Pass 1 Table (Masiero et al., 2011). For both asteroids we assumed a constant spectral emissivity of 0.9. Our NEATM results (Fig. 3) for (90) Antiope indicate a diameter, $D = 111.5 \pm 1.4$ km, an albedo, pv = 0.07 ± 0.01, and a beaming parameter, $\eta = 0.90 \pm 0.01$. Spitzer was not able to resolve both Antiope and its companion, although the Wide-field Infrared Survey Explorer (WISE) was successful in doing so. Instead of reporting the WISE values (Masiero et al., 2011) for Antiope and its companion independently, we averaged them, comparing this average with our Spitzer results. The average WISE $D = 121.2 \pm 2.5$, pv = 0.06 ± 0.01, and $\eta = 0.94 \pm 0.01$. The diameter and eta result are slightly higher than ours even provided the errors, but are still very consistent. Our NEATM results

[4] http://ssd.jpl.nasa.gov/horizons.cgi.

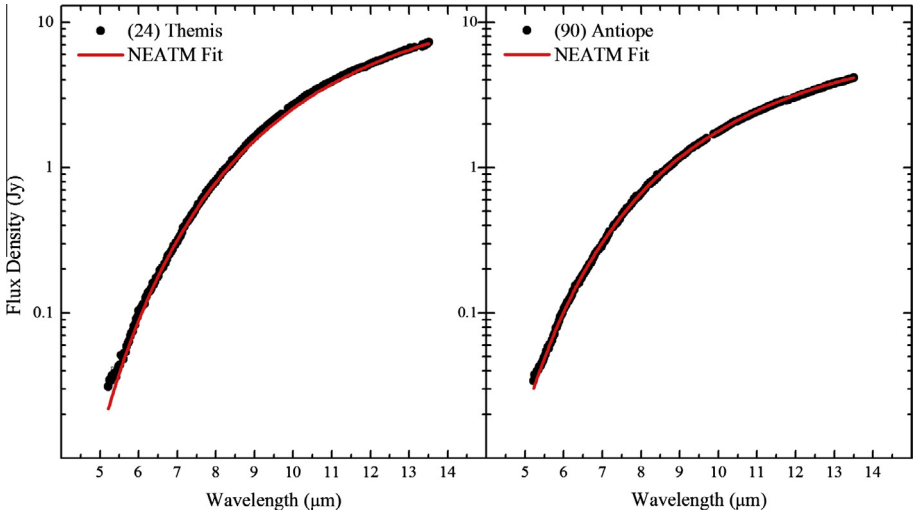


**Fig. 3.** Mid-infrared flux density spectra of (24) Themis and (90) Antiope acquired by the Spitzer Space Telescope. The red solid line indicates the best-fit NEATM result. (For interpretation of the references to color in this figure legend, the reader is referred to the web version of this article.)

for (24) Themis indicate a $D = 218 \pm 1$ km, pv = $0.06 \pm 0.01$, and $\eta = 1.15 \pm 0.01$. Our values are similar to that found by Lim et al. (2005), who determined a $D = 210 \pm 14$, and $\eta = 0.90 \pm 0.07$, assuming an albedo of 0.07 and spectral emissivity of 0.98.

## 5. Emissivity spectrum

In the mid-infrared, asteroid surface spectroscopy is dominated by thermal emission, which is affected by the composition and grain structure (size, porosity) of the surface. To reveal small-scale absorption features or emission features in the thermal emission spectra, we divided the Spitzer mid-infrared spectra of Asteroid (24) Themis and (90) Antiope by their thermal continuum model computed by the NEATM. Any deviations from the theoretical model are potentially spectral features, useful for comparison with other asteroids as well as interpreting surface minerals. Two such indicators of mineralogy in the mid-IR are the Si–O stretch and bend fundamentals located between ~8.2–12.5 μm and ~14–25 μm, respectively. The Si–O stretch is the strongest vibrational mode of silicates caused by the asymmetric displacement of the oxygen in the Si–O bonds (Jones, 1988). Combined with the Si–O bend, these fundamental molecular vibrations give rise to the 10-μm and 20-μm emission plateaus that are an important marker of asteroid composition. The spectral contrast of the silicate emission features is also diagnostic of an asteroid's surface structure (under-dense or compact) as well as grain size. For example, Trojan asteroids are relatively featureless in the visible and near-infrared, yet these objects have compositionally-detailed, high-contrast 10-μm and 20-μm emission features in the mid-infrared. This lack of information in reflectance spectra and presence in thermal emission spectra may be due to grain sizes less than 2 μm, first suggested by Emery et al. (2006) and later refined by Vernazza et al. (2012).

In Fig. 4 we show the 8.2–12.5-μm emissivity spectra of (90) Antiope and (24) Themis. The longer wavelength data for Antiope (up to ~37 μm) were obtained by Spitzer, but do not include the observations necessary for background subtraction of the SH and LH modules (see Section 2.2 for details). Optimally we would like to interpret the 8–37-μm emission spectrum of Antiope since any emission features from silicates at these longer wavelengths can strengthen our interpretation of features produced by these same minerals at shorter wavelengths. In the absence of Antiope's full emission spectrum, we will limit our analysis to the 8.2–12.5-μm region, and our interpretations will require confirmation from data at longer wavelengths when these become available.

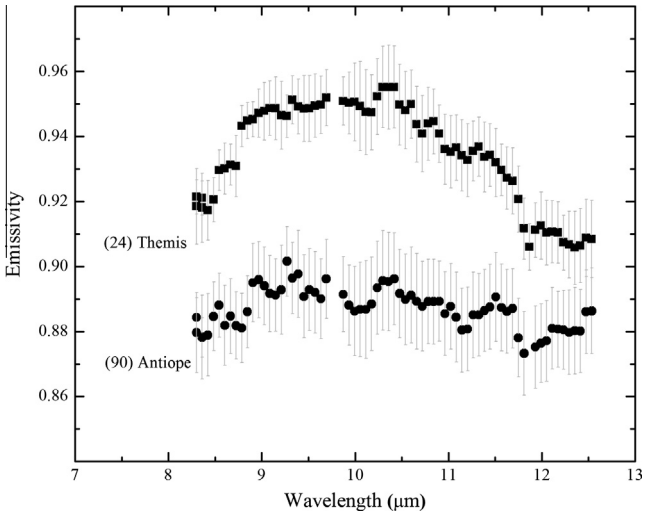


**Fig. 4.** Emission spectra of (24) Themis and (90) Antiope. In the 8.2–12.5-μm region (24) Themis shows an emission feature roughly 5% in strength that arises from small-grain silicates in a fluffy, under-dense regolith. In the same region (90) Antiope does not appear to have a broad emission feature. The absence of this broad emission in Antiope's spectrum is likely due to larger surface grains and/or lower surface porosity.

The emission spectrum of Themis has an overall broad, rounded bump between 8.3 and 12.0 μm that rises from 8.3 μm to 9.0 μm, plateaus from this point until 10.3 μm, and then steadily declines to a minimum around 12.0 μm. We consider this asteroid to have a low-contrast 10-μm silicate emission of roughly 5%, and this is consistent with a study of eight other Themis-family asteroids, all characterized with an emission strength of approximately 5% (Licandro et al., 2012). Antiope's emission spectrum does not show a broad overall bump as in the case of Themis; rather, it peaks around 9.3 μm and steadily declines to approximately 11.8 μm.

The spectral contrast of the 10-μm silicate emission for both asteroids suggests differences in their surface structures from those of comets and Trojan asteroids. Antiope has a surface structure that is the least consistent with these objects, while Themis may have a surface intermediary between them. The high contrast 10-μm silicate emission "bump" in the spectra of Trojan asteroids

were found by Vernazza et al. (2012) to be the result of small grains on the first millimeter of the surface that produces a high porosity "fluffy" surface. It is possible that Themis and Antiope have larger surface grains, and thus lower surface porosity than the Trojans. Larger grain sizes could also be a consequence of lower gravity, making these asteroids less likely to retain finer dust particles. On the other hand, Trojan Asteroid (624) Hektor has a diameter of roughly 225 km, similar to (65) Cybele, yet has an emission strength double that of Cybele (Emery et al., 2006). We do not attribute the strength of the 10-μm emission to diameter alone. We propose that aqueous alteration processes that produced visible and near-infrared hydration features in some asteroids may also affect their surface porosities or grain sizes, and thus the spectral contrast of their 10-μm feature. For example, Asteroid (65) Cybele was shown by Licandro et al. (2011) to have a rounded water–ice absorption at 3.1 μm, and a 10-μm silicate emission on the order of ~5%. Cybele Asteroid (107) Camilla was found by Hargrove et al. (2012) to exhibit a similar water–ice absorption at 3.1 μm, and had a 10-μm silicate emission of approximately 5%. Hargrove et al. (2012) also found Binary-Cybele Asteroid (121) Hermione to exhibit a sharp 3-μm OH feature, with no 10-μm emission in the ~8–12-μm region. These lower contrast, rounded 10-μm silicate emission features (0–5%) could be a trend amongst asteroids with hydroxyl or water–ice absorptions in the 3-μm region, but more observations of asteroids with these features are needed in the mid-infrared.

## 6. Conclusions

We present near-infrared 2–4-μm spectra of Themis-family binary Asteroid (90) Antiope. We report the presence of a 3-μm feature, most likely a rounded 3.1-μm feature, in our (90) Antiope spectra. The shape of the 3.1-μm feature is qualitatively similar to that produced by $H_2O$ ice that Campins et al. (2010) and Rivkin and Emery (2010) detected in the spectrum of the largest family member (24) Themis. The possible presence of water ice is consistent with at least four Main Belt comets in this family (or the Beagle sub-family; e.g. Haghighipour, 2009; Hsieh et al., 2012; Hsieh, 2014), and the models of Castillo-Rogez and Schmidt (2010).

In the mid-infrared we find that there may exist variations in the surface structure of Asteroids (24) Themis and (90) Antiope from our analysis of their Spitzer IRS spectra. The 8.2–12.5-μm emissivity spectra of (90) Antiope and (24) Themis are different in contrast and shape. Antiope's spectrum is relatively flat with no apparent 10-μm silicate emission, indicating that this object likely does not have a fluffy, "fairy castle" type surface structure that produces the broad, high contrast (10–15%) silicate emission plateau in Trojan asteroids (Emery et al., 2006) and comets (e.g. Harker et al., 2005). The 8–12-μm emission spectrum of Antiope is comparable to that seen in our recent work with Cybele Asteroid (121) Hermione (Hargrove et al., 2012). In this same 8.2–12.5-μm region, (24) Themis exhibits a rounded 10-μm emission roughly 5% in strength, more similar to other Themis-family Asteroids (Licandro et al., 2012), (65) Cybele (Licandro et al., 2011), and (107) Camilla (Hargrove et al., 2012). Compared to Trojans and comets, the lower contrast (0–5%) emission spectra of both Antiope and Themis, respectively, may indicate larger grain silicates are present on the surfaces of these asteroids and/or lower surface porosities. We suggest these differences in surface structure, apparent in the mid-infrared, are the result of aqueous processes that produced their near-infrared 3-μm features, and possible 0.7-μm feature in the case of (90) Antiope.

More 2–4-μm investigations of primitive, outer-belt objects are needed, especially for the Themis family. Thus far, only three asteroids in the Themis family have been observed in this diagnostic region. Asteroid (24) Themis shows strong evidence of surface water ice, while our detection of ice on (90) Antiope is only tentative due to the low $S/N$ of our data sets. Asteroid (104) Klymene shows signs of aqueous alteration in the form of a sharp 3-μm feature (Takir and Emery, 2012) and is the only member of this family thus far to exhibit this absorption. Perhaps (104) Klymene and (90) Antiope represent different compositional regions of the parent body or experienced variations in thermal processing. Understanding the diversity of aqueous and thermal processing within the Themis family is important for geophysical evolution models of volatile-rich asteroid families (e.g. Castillo-Rogez and Schmidt, 2010) and dynamical models of the Solar System (e.g. Walsh et al., 2011).

## Acknowledgments

Kelsey Hargrove gratefully acknowledges support from support from NASA's Graduate Student Research Program (GSRP), and Humberto Campins from the National Science Foundation and NASA. Joshua P. Emery gratefully acknowledges support from NASA Planetary Astronomy grants NNX08AV93G and NNX14AJ39G. This work is based in part from archival data obtained by the Spitzer Space Telescope. The Spitzer Space Telescope, which is operated by the Jet Propulsion Laboratory, California Institute of Technology under a contract with NASA. Our 2–4-μm data were obtained with NASA's Infrared Telescope Facility, which is operated by the University of Hawaii under Cooperative Agreement No. NNX-08AE38A with the National Aeronautics and Space Administration, Science Mission Directorate, Planetary Astronomy Program. The 0.4–2.5-μm data we show in Fig. 2 were obtained and made available by the MIT-UH-IRTF Joint Campaign for NEO Reconnaissance. The MIT component of this work is supported by NASA Grant 09-NEOO009-0001, and by the National Science Foundation under Grants Nos. 0506716 and 0907766.

## References

Bowell, E. et al., 1989. Application of photometric models to asteroids. In: Binzel, R.P., Gehrels, T., Matthews, M.S. (Eds.), Asteroids II. University of Arizona Press, Tucson, AZ, pp. 524–556.
Bus, S.J., Binzel, R.P., 2002. Phase II of the small main-belt asteroid spectroscopic survey – A feature-based taxonomy. Icarus 158, 146–177.
Campins, H. et al., 2010. Water ice and organics on the surface of the Asteroid 24 Themis. Nature 464, 1320–1321.
Castillo-Rogez, J.C., Schmidt, B.E., 2010. Geophysical evolution of the Themis family parent body. Geophys. Res. Lett. 37, L10202.
Cushing, M.C., Vacca, W.D., Rayner, J.T., 2004. Spextool: A Spectral Extraction Package for SpeX, A 0.8–5.5 micron Cross-dispersed Spectrograph. Astron. Soc. Pacific 116, 362–376.
De Leon, J. et al., 2012. Near-infrared spectroscopic survey of B-type asteroids: Compositional analysis. Icarus 218, 196–206.
de Strobel, G.C., 1996. Stars resembling the Sun. Astron. Astrophys. Rev. 7, 243–288.
DeMeo, F. et al., 2009. Asteroid Taxonomy V1.0. NASA Planetary Data System, p. 114.
Descamps, P. et al., 2007. Figure of the double Asteroid 90 Antiope from adaptive optics and lightcurve observations. Icarus 187, 482–499.
Descamps, P. et al., 2009. A giant crater on 90 Antiope? Icarus 203, 102–111.
Emery, J.P., Cruikshank, D.P., Van Cleve, J., 2006. Thermal emission spectroscopy (5.2–38 μm) of three Trojan asteroids with the Spitzer Space Telescope: Detection of fine-grained silicates. Icarus 182, 496–512.
Florczak, M. et al., 1999. A spectroscopic study of the Themis family. Astron. Astrophys. Suppl. Ser. 134, 463–471.
Fornasier, S. et al., 2014. Aqueous alteration on Main Belt primitive asteroids: Results from visible spectroscopy. Icarus 233, 163–178.
Haghighipour, N., 2009. Dynamical constraints on the origin of Main Belt comets. Meteorit. Planet. Sci. 44, 1863–1869.
Hargrove, K.D. et al., 2012. Asteroids (65) Cybele, (107) Camilla and (121) Hermione: Infrared spectral diversity among the Cybeles. Icarus 221, 453–455.
Harker, D.E., Woodward, C.E., Wooden, D.H., 2005. The dust grains from 9P/Tempel 1 before and after the encounter with Deep Impact. Science 310, 278–280.
Harris, A.W., 1998. A thermal model for near-Earth asteroids. Icarus 131, 291–301.
Houck, J.R. et al., 2004. The Infrared Spectrograph (IRS) on the Spitzer Space Telescope. Astrophys. J. Suppl. Ser. 154, 18–24.
Howell, E.S. et al., 2011. Hydrated silicates on main-belt asteroids: Correlation of the 0.7- and 3-micron absorption bands. EPSC Abstracts 6, p. 637.

Hsieh, Henry H., 2014. The nucleus of main-belt Comet P/2010 R2 (La Sagra). Icarus 243, 16–26.
Hsieh, H.H. et al., 2012. Discovery of main-belt Comet P/2006 VW139 by Pan-STARRS1. Astrophys. J. 748, L15.
Jones, T.D., 1988. An Infrared Reflectance Study of Water in Outer Belt Asteroids: Clues to Composition and Origin. Ph.D. Thesis, Univ. Arizona.
Lazzaro, D. et al., 2004. S3OS2: The visible spectroscopic survey of 820 asteroids. Icarus 172, 179–220.
Lebofsky, L.A., Spencer, J.R., 1989. Radiometry and a thermal modeling of asteroids. In: Binzel, R.P., Gehrels, T., Matthews, M.S. (Eds.), Asteroids II. Univ. Arizona Press, Tucson, AZ, pp. 128–147.
Licandro, J. et al., 2011. (65) Cybele: Detection of small silicate grains, water–ice, and organics. Astron. Astrophys. 525, A34.
Licandro, J. et al., 2012. 5–14 μm Spitzer spectra of Themis family asteroids. Astron. Astrophys. 537, A73.
Lim, L.F. et al., 2005. Thermal infrared (8–13 μm) spectra of 29 Asteroids: The Cornell mid-infrared asteroid spectroscopy (MIDAS) survey. Icarus 173, 385–408.
Lord, S.D., 1992. A new software tool for computing Earth's atmospheric transmission of near- and far-infrared radiation. NASA Technical Memorandum, 103957, 1.
Marchis, F. et al., 2011. The origin of (90) Antiope from component-resolved near-infrared spectroscopy. Icarus 213, 252–264.
Masiero, J.R. et al., 2011. Main Belt asteroids with WISE/NEOWISE. I. Preliminary albedos and diameters. Astrophys. J. 741, 68.
Mothé-Diniz, T., Roig, F., Carvano, J.M., 2005. Reanalysis of asteroid families structure through visible spectroscopy. Icarus 174, 54–80.
Rayner, J.T., Toomey, D.W., Onaka, P.M., 2003. SpeX: A medium-resolution 0.8–5.5 micron spectrograph and imager for the NASA Infrared Telescope Facility. Astron. Soc. Pacific 115, 362–382.
Rivkin, A.S., Emery, J.P., 2010. Detection of ice and organics on an asteroidal surface. Nature 464, 1322–1323.
Rivkin, A.S. et al., 2002. Hydrated minerals on asteroids: The astronomical record. In: Bottke, W.F., Cellino, A., Paolicchi, P., Binzel, R.P. (Eds.), Asteroids III. University of Arizona Press, Tucson, AZ, pp. 235–253.
Takir, D., Emery, J.P., 2012. Outer Main Belt asteroids: Identification and distribution of four 3-μm spectral groups. Icarus 219, 641–654.
Tholen, D.J., Barucci, M.A., 1989. Asteroid taxonomy. In: Binzel, R.P., Gehrels, T., Matthews, M.S. (Eds.), Asteroids II. Univ. Arizona Press, Tucson, AZ, pp. 298–315.
Vernazza, P. et al., 2012. High surface porosity as the origin of emissivity features in asteroid spectra. Icarus 221 (2), 1162–1172.
Vilas, F., 1994. A cheaper, faster, better way to detect water of hydration on Solar System bodies. Icarus 111, 456–467.
Vilas, F. et al., 1993. CCD reflectance spectra of selected asteroids. II. Low-albedo asteroid spectra and data extraction techniques. Icarus 105, 67–78.
Walsh, K.J. et al., 2011. A low mass for Mars from Jupiter's early gas-driven migration. Nature 475, 206–209.
Werner, M.W., Roellig, T.L., Low, F.J., 2004. The Spitzer Space Telescope mission. Astrophys. J. 154, 1–9.
Zappala, V. et al., 1995. Asteroid families: Search of a 12,487-asteroid sample using two different clustering techniques. Icarus 116, 291–314.
Ziffer, Julie. et al., 2011. Near-infrared spectroscopy of primitive asteroid families. Icarus 213, 538–546.